Electron Photodetachment from Gas Phase Peptide Dianions. Relation with Optical Absorption Properties

Laure Joly,[†] Rodolphe Antoine,*[,†] Michel Broyer,[†] Jérôme Lemoine,[‡] and Philippe Dugourd[†]

Université de Lyon, Université Lyon 1, CNRS, LASIM UMR 5579, bât. A. Kastler, 43 Bvd. du 11 novembre 1918, 69622 Villeurbanne, France, and Université de Lyon, Université Lyon 1, CNRS, Sciences Analytiques, UMR 5180, 43 Bvd. du 11 Novembre 1918, 69622 Villeurbanne cedex, France

Received: July 5, 2007; In Final Form: November 9, 2007

Electron detachment from peptide dianions is studied as a function of the laser wavelength. The first step for the detachment is a resonant electronic excitation of the dianions. Electronic excitation spectra are reported for three peptides, including gramicidin. A comparative study of the detachment yield for 13 peptides was performed at 260 nm and at 220 nm. At 260 nm, the detachment yield is mainly driven by the sum of the absorption coefficients of the aromatic amino acids that are contained in the peptide. At 220 nm, no direct relation is observed between the electron photodetachement yields and the sum of absorption efficiencies. At this wavelength, the sequence and the structure of the peptide may have an influence on the photodetachment process.

I. Introduction

Multiply charged anions (MCAs) are ubiquitous species encountered in solution and solid states. Their study in the gas phase provides new opportunities to address some fundamental questions about their intrinsic properties and the role of solvation or counterions in their stability.[1−5] In particular, MCAs in the gas phase present specific properties with respect to the electron detachment as compared to singly charged anions. The superposition of the short-range binding of the electron and the long-range Coulomb repulsion gives rise to a repulsive Coulomb barrier (RCB) that can trap excess electrons. Electron detachment can then occur through electron tunneling. High barrier can also stabilize metastable anions with negative electron binding energy.[6,7] Direct measurements of the excess electron binding energy and the RCB of MCAs are provided by the combination of photoelectron spectroscopy and mass spectrometry.[8] Electron tunneling has also been investigated by photon energy dependent studies.[9,10]

Proteins and DNAs can be easily transferred to the gas phase with a high charge state by electrospray[11,12] and can be used as prototypes to study detachment mechanisms in highly charged anions and also the influence of the molecular flexibility on detachment.[13,14] Gas phase MCAs of DNA have driven many interests[7,15] in relation with their redox properties and with photoinduced damages in solution. Recently, we performed energy-resolved spectroscopy experiments on gas phase MCAs of DNAs.[16,17] We observed electron detachment and showed that this detachment was strongly base dependent.

Surprisingly, few works have been performed on MCAs of polypeptides. Doubly deprotonated peptides are subjected to electron detachment when irradiated by a UV light.[18] The electron detachment yield was used to monitor the excited electronic spectrum of the trapped ions[18,19] as recently illustrated by the first measurement of the electronic excited spectrum of a gas phase protein.[20]

* Corresponding author. E-mail: rantoine@lasim.univ-lyon1.fr.
[†] CNRS, LASIM UMR 5579.
[‡] CNRS, Sciences Analytiques.

TABLE 1: Summary of the Peptide Sequences

notation	sequence	name
P1	SDRGDGG	
P2	RRRADDSDDDDD	
P3	RGDSPASSKP	
P4	EGVNDNEEGFFSAR	fibrinopeptide B human
P5	RPPGFSPFR	
P6	RPKPQQFFGLM-NH_2	Substance P
P7	DYKDDDDK	
P8	DRVYVHPF	angiotensin II [val^5]
P9	pyro-ELYENKPRRPYIL	neurotensin
P10	CYIQNCPLG-NH_2	oxytocin
P11	Boc-β-AWMDF-NH_2	pentagastrin
P12	WYGGWYGGWY	
P13	formyl-VGALAVVVWLWLWLW-ethanolamine	gramicidin A

In this paper, we aim at evaluating the influence of the sequence of the peptide and of the laser wavelength on the electron detachment yield, which is a first step toward the interpretation of electron detachment processes in MCA polypeptides. We present a detailed study of electron photodetachment on a panel of peptide dianions. The parameters that govern electron detachment, in particular the influence of the photon energy with respect to the binding energy and the repulsive Coulomb barrier, will be discussed.

II. Experimental Section

Sample Preparation. Peptides, whose sequences are listed in Table 1, were purchased from commercial sources (Sigma-Aldrich and Bachem). They were dissolved at a concentration of 100 μM in H_2O/CH_3CN (50/50, v/v) and directly electrosprayed.

Mass Spectrometry, Laser Irradiation of Trapped Ions, and UV/Vis Absorption. The experimental setup[21] consists of a commercial LCQ Duo quadrupole ion trap mass spectrometer (ThermoFinnigan, San Jose, CA) coupled to a Panther OPO laser pumped by a 355 nm Nd:YAG PowerLite 8000 (5 ns pulse width, 20 Hz repetition rate). Frequency doubling allows scanning in the 215−330 nm range. The vacuum chamber and

10.1021/jp0752365 CCC: $40.75
Published on Web 01/16/2008

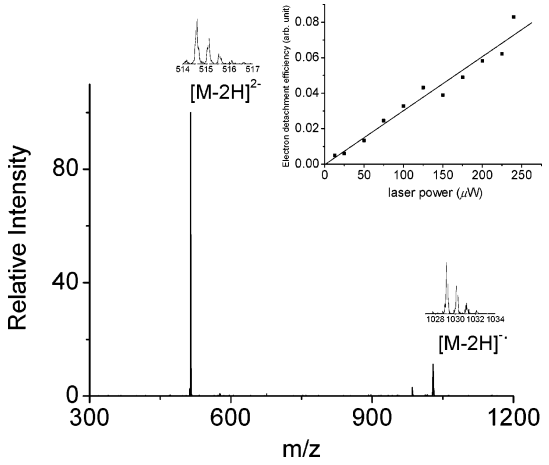

Figure 1. Mass spectrum obtained after laser irradiation ($\lambda = 260$ nm) of the doubly deprotonated angiotensin II [val^5] peptide ion precursor (sequence DRVYVHPF). The irradiation time was 500 ms. The inset shows the detachment yield ($\ln((I_{[M-2H]^{2-}} + I_{[M-2H]^{-}})/I_{[M-2H]^{2-}})$) measured as a function of the laser power at $\lambda = 260$ nm. The experimental zoom scans recorded for the $[M - 2H]^{2-}$ and $[M - 2H]^{-\bullet}$ ions are also shown.

the central ring electrode of the mass spectrometer were modified to allow the injection at the center of the trap of UV and visible lights. An electromechanical shutter triggered on the RF signal of the ion trap synchronizes the laser irradiation with the trapping of the ions. The ions are injected into the trap, mass selected, and then laser-irradiated. Fragmentation spectra are systematically recorded as a function of the laser wavelength. The photodetachment yield is given by, ln((parent + fragment)/parent)/λ/P_l where λ is the laser wavelength and P_l is the laser power.

UV−vis spectra in solution were recorded using an AvaSpec-2048 Fiber optic spectrometer, an AvaLight-DH−S deuterium-halogen light source, and a UV−vis cuvette by Avantes.

Molecular Dynamics Simulations. One of the goals of this paper is to study the influence of the repulsive Coulomb interaction between negative charges on the electron detachment. The dynamical motions of the doubly deprotonated peptides, at 300 K, cause the distance R among the negatively charged units to fluctuate. MD simulations were carried out to estimate this distance and the Coulomb interaction. Molecular dynamics (MD) trajectories were obtained using the DYNAMICS program, which is a part of the software TINKER package.[22] The simulations were run in vacuum with the dielectric constant set at 2 and temperature at 350 K. The MD simulations were carried out using Amber with the parm99 all atom force field using the weak-coupling Berendsen method.[23] Initial structures (extended conformation) were first subjected to a short minimization to remove bad steric contacts and were thermalized for 50 ps for peptides P1 and P8 and 100 ps for peptide P4. A total of 1500 ps simulations were performed with a 1 fs step. We collected the Coulomb repulsion energy $e^2/R = (14.4 \text{ eV})/[R (\text{Å})]$, where R is the distance between the two negative charges, every 0.1 ps (100 steps). Note that we assume that each carboxylate carries a full −1 charge and ($\epsilon = 1$) when evaluating the Coulomb potential. A histogram of the Coulomb repulsion between the deprotonated sites can be obtained after the MD run. This histogram gives the number of events in which a given value of the Coulomb potential is realized (see below).

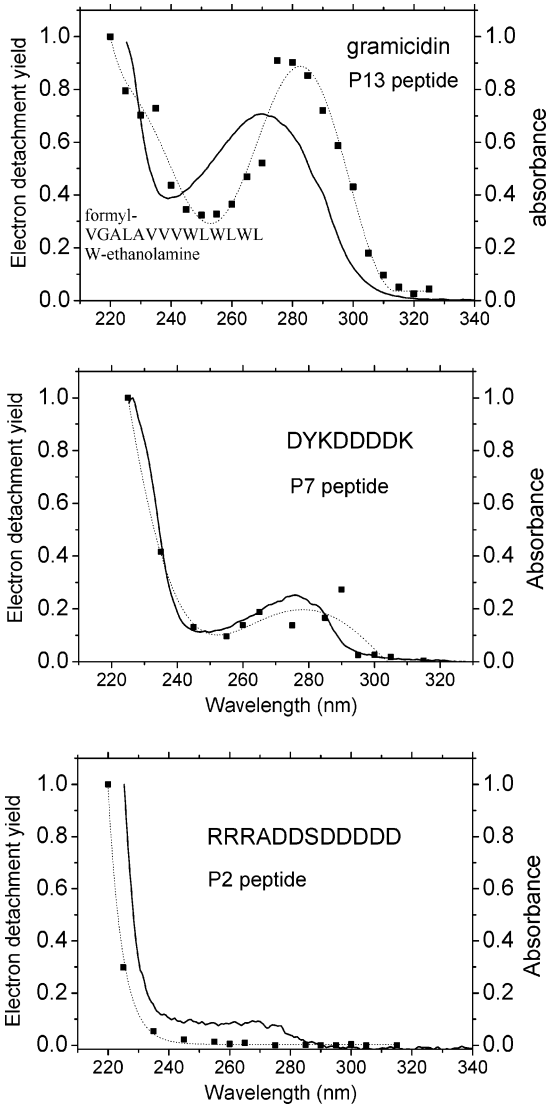

Figure 2. (■) Normalized photodetachment yield as a function of the wavelength for the doubly deprotonated $[M - 2H]^{2-}$ ions of gramicidin (formyl-VGALAVVVWLWLWL-ethanolamine) (a), peptide DYKDDDDK (b), and peptide RRRADDSDDDDD (c). Dashed curves are smoothed curves of the experimental photodetachment yields. The irradiation time was 500 ms. Solid lines show the normalized absorption spectra of the peptides in solution (100 μM of peptides in H_2O/CH_3CN (50/50, v/v)).

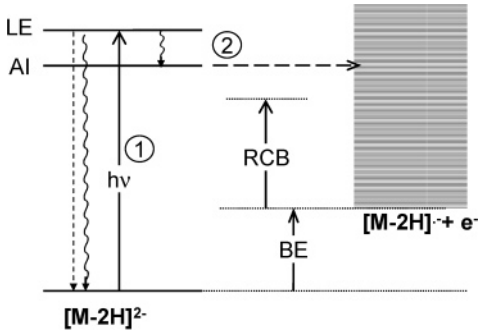

Figure 3. Two-step mechanism for electron photodetachment in peptide dianions: (1) electronic excitation of a chromophore (local excitation; LE); (2) crossing with an autoionizing state (AI) and detachment of the electron.

MD simulations were performed for peptides P1, P4, and P8 with several different initial extended structures. MD simulations

SCHEME 1: Proposed Mechanism for the Loss of CO_2 (−44 Da) from the$[M - 2H]^{-\bullet}$ Anion

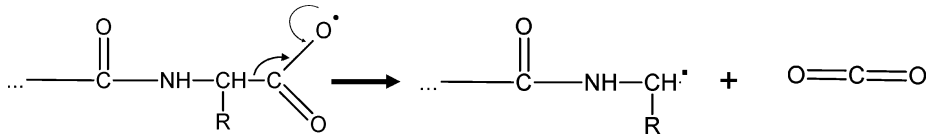

were performed with different initial structures and lead qualitatively to similar trends.

III. Results and Discussion

Photodetachment Spectra in the Gas Phase versus Absorption Spectra in Solution. The mass spectrum obtained following the UV laser irradiation at 260 nm of the doubly deprotonated P8 peptide (DRVYVHPF) is shown in Figure 1. The main fragment observed at *m*/*z* 1029 corresponds to the oxidized $[M - 2H]^{-\bullet}$ ion generated by electron detachment from the $[M - 2H]^{2-}$ precursor ion. This photoinduced charge reduction from the precursor ion is the main fragment channel observed for every peptide dianions used in this study. Another fragment observed at *m*/*z* 985 is due to the loss of CO_2 (−44 Da) from the $[M - 2H]^{-\bullet}$ anion (see Scheme 1).

Experiments performed at 260 nm as a function of the laser power show that this charge reduction is a one-photon process (as shown in inset of Figure 1 for P8 peptide).[18]

The influence of the laser wavelength was also investigated. Figure 2 presents the electron photodetachment efficiency as a function of the wavelength for three peptides. The detachment yield curve shows a strong dependence of the electron detachment events with the laser wavelength. The detachment is observed in the region where the absorption occurs in solution (also displayed in Figure 2). In particular, for peptides P7 (DYKDDDDK) and P13 (formyl-VGALAVVVWLWLWLW-ethanolamine), which possess respectively one and four aromatic amino acids, the electron detachment is observed below 300 nm in the wavelength range where $\pi-\pi^*$ transitions of aromatic residues occur. On the other side, for peptide P2 (RRRADDSDDDDD), which does not possess aromatic amino acid, the electron detachment is only observed below 240 nm, which corresponds to the emergence of the *n* to π^* and π to π^* transitions in the peptide backbone.[24] This spectrum shows that it is possible to efficiently detach electron even for peptides that do not contain chromophores. In Figure 2, the small shifts observed between gas phase and solution spectra illustrate the effect of the environment. In particular, the band at 280−300 nm is red-shifted for gas phase gramicidin and (in a lesser extent) for peptide P7 as compared to solution spectra.

Energetic Considerations. These results (power and wavelength dependences) show that the first step in the electron detachment is a resonant electronic excitation. The π^* state is a bound state and the ionization energy of the aromatic residue (∼8.49 eV for the phenol) is well above the photon energy (4.66 eV at 260 nm) which should prevent a direct decay from the π^* state to the photodetached continuum. The decay might occur through a two electron process whereby the π^* electron fall back into the π hole and transfer its energy to a more weakly bound electron that can be ejected to the continuum. Another possibility is that the nuclear motion in the $\pi\pi^*$ excited state leads to a curve crossing a different state that autoionizes (as illustrated in Figure 3). Without time-resolved experimental data or theoretical modeling, it seems speculative to decide between these mechanisms. Obviously, this detachment may be influenced by the value of the photon and of the autoionizing state energies with respect to the binding energy (BE) and the

SCHEME 2: Schematic Energy Diagram Showing (a) the Excess Electron Binding Energy (BE_1) without Barrier for Singly Deprotonated Anion $[M - H]^-$, (b) the Excess Electron Binding Energy (BE_2) with the Repulsive Coulomb Barrier (RCB) for Doubly Deprotonated Anion $[M - 2H]^{2-}$ [a]

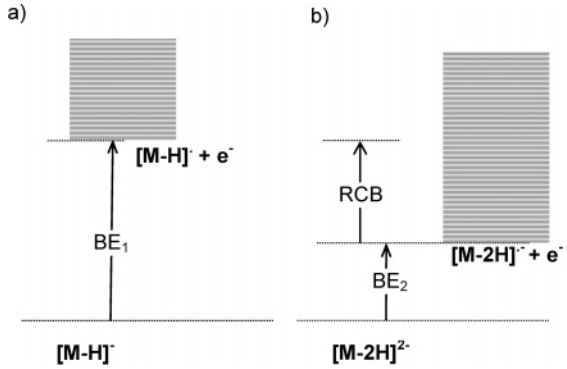

[a] $BE_1 = RCB + BE_2$ is assumed (see refs 8 and 13).

repulsive Coulomb barrier (see Figure 3). In particular, if the photon energy brings the peptide dianion into an electronic excited state, which is higher than the ground state energy of $[M - 2H]^{-\bullet}$ species, but lower than the barrier (RCB > $h\nu$ > BE), electron detachment from the excited state occurs by tunneling through the barrier. Tunneling efficiency depends on the width of the barrier, which depends on the stability of the radical. Electron tunneling through repulsive Coulomb barriers has been reported, for example, for linear dicarboxylate dianions.[9]

In a peptide dianion, the negative charges are localized on acidic residues (in particular on carboxyl groups beared by the peptide C-terminal and side chains of the acidic aspartic and glutamic amino acids). An estimation of the binding energy of the electron at the C-terminal carboxylate can be obtained from photoelectron spectroscopy of the $HCOO^-$ anion. An electron affinity of 3.498 eV was determined.[25] Adiabatic detachment energy for $HCOO^-$ was calculated using density functional theory (DFT) with the B3LYP hybrid functional and the aug-cc-pvdz basis set. The calculated value is 3.49 eV in close agreement with experimental value. The same calculation provides a value of 3.79 eV for the binding energy of an electron at the deprotonated carboxylic side chain of the aspartic amino acid. For a dianion, the binding energy is reduced by the repulsion $e^2/R = (14.4\text{ eV})/[R\text{ (Å)}]$ between the two charges. The RCB is equal to the same value $e^2/R = (14.4\text{ eV})/[R\text{ (Å)}]$ (as depicted in Scheme 2).

To estimate the RCB, we have carried out molecular dynamics simulations for peptides P1, P4, and P8, which vary from 7 to 14 amino acids in size. For these calculations, the charges were localized on the sequence according to the pK_a values of the different acidic groups containing peptides. For peptide P1, we localized the two negative charges on the carboxyl groups of asp[2] and C-terminal. For peptides P4 and P8, charges were localized respectively on asp[5] and C-terminal, and asp[1] and C-terminal. During the MD simulations, the geometrical fluctuations result in changes in the distance

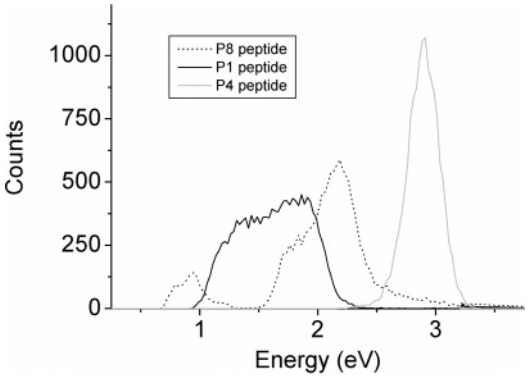

Figure 4. Distribution of the Coulomb repulsion energy between the two deprotonated sites. Each histogram is obtained from a 1500 ps MD simulations. The sampling time is 0.1 ps.

between the two charge sites, inducing fluctuation of the Coulomb repulsion energies. The distribution of the values for the Coulomb potential values, obtained during the MD simulations for the three peptides are plotted in Figure 4. The Coulomb energies oscillate between 0.5 and 3.5 eV. The widths and the maxima of the distribution are strongly peptide dependent. The maxima of the distribution are for peptide P1 ~1.8 eV, for P8 ~2.2 eV, and for P4 ~2.9 eV. The evolution of the maximum is correlated to the number of amino acids between the two charges in the peptide. In peptide P4 there are 9 amino acids between the two negative charges whereas for peptides P1 and P8, there are respectively 5 and 6 amino acids between charges. This evolution may be explained by the fact that a high number of amino acids between charges allow a better charge solvation leading to structures with shorter distances between charges. A more plausible explanation would perhaps be that the longer molecule could more easily fold back on itself leading to shorter distances between the charge centers. We tested this by doing the same simulation on P8 without the charges. We see that the relative distances between the amino acids has qualitatively the same trend as in the case of the charged systems. The conclusions of these energetic considerations are the following:

(i) The fluctuations in the RCB imply that the binding energy depends on the conformation of the peptide.

(ii) There is a very low probability of observing a Coulomb potential above ~3.5 eV. Thus these peptide dianions possess a positive binding energy and are stable in the gas phase. Consequently, thermal electron detachment is expected to be negligible which is confirmed experimentally in our observation time window.

(iii) The excitation with a UV light in the 220−330 nm range leads to an increase in the internal energy of the peptide of 3.76−5.64 eV. This energy range is above the binding energy of the electron plus the RCB. If the energy of the autoionizing state is close to the photon energy, electron detachment does not imply tunneling through the RCB (as illustrated in Figure 3), and thus conformation fluctuations have a weak influence on the photodetachment process contrary to what was observed for DNA strands.[13,26]

Here we want to emphasize the difference of mechanisms for the electron photodetachment between peptide and oligonucleotide polyanions. For oligonucleotides, the charges are carried by the phosphates. The electron binding energy of $H_2PO_4^-$ is ~5 eV.[27] This binding energy is higher than the binding energy of carboxylate on peptides (~3.5 eV). For DNAs, the excitation with a UV light in the 220−330 nm range leads to an increase in the internal energy that is below the RCB. Thus, for oligonucleotides, the detachment of an electron occurs by tunneling through the RCB. This step depends on the stability of the radical and on the IP of the excited base.[17]

Relation between Electron Photodetachment and Absorbance at 260 and 220 nm. Because, for peptides, the electron photodetachment is a two-step mechanism which does not involve tunneling through RCB, one may expect that the first step depending on the absorption properties of the peptide will drive the detachment yield. Thus, the electron photodetachment yield $P_i = \ln((\text{parent} + \text{fragment})/\text{parent})$ can be compared to the absorbance A_i of the peptides defined by

$$A_i = C\epsilon_{\text{peptide}}^{\lambda_i} \tag{1}$$

where $\epsilon_{\text{peptide}}^{\lambda_i}$ is the extinction coefficient of peptides at the λ_i wavelength. C is a normalization constant. For a given wavelength, C was chosen to minimize

$$Q = \sqrt{\sum_i (C\epsilon_{\text{peptide}}^{\lambda_i} - P_i)^2} \tag{2}$$

where the sum on the index i is over the molecules considered. At 260 nm, the optical absorption of peptides is mainly given by the absorption of their aromatic amino acid residues. The extinction coefficients of peptides may thus be approximated by

$$\epsilon_{\text{peptide}}^{260\text{nm}} = \sum_i^{\text{Trp,Tyr,Phe}} \epsilon_i^{260\text{nm}} \tag{3}$$

Figure 5a compares the electron photodetachment yield P_i performed at 260 nm for 13 peptides (listed in Table 1) with their absorption properties estimated by eq 3 and their extinction coefficients listed in Table 2. Except for oxytocin (peptide P10), an overall good agreement is obtained ($Q = 0.913$). In particular, the peptides without chromophores do not present significant electron detachment whereas the peptides containing a high number of tryptophan, such as peptide P12 and gramicidin A (peptide P13) display an efficient electron detachment. Concerning oxytocin, the two cysteines are linked by a disulfide bridge which is characterized by a significant absorption around 260 nm[28] that was not taken into account in eq 3. Furthermore, one of the deprotonation sites occurs on the tyrosine side chain leading to a phenoxide anion known to have a low binding energy (2.253 eV).[29] The low binding energy of the negative charge on the tyrosylate residue close to the excitation site may enhance electron detachment.

At 220 nm, the optical absorption of peptides is due to the emergence of the n to π^* and π to π^* transitions in the peptide backbone and aromatic side chains. The extinction coefficients of peptides may be crudely approximated by

$$\epsilon_{\text{peptide}}^{220\text{nm}} = n\,\epsilon_{\text{peptide bond}}^{220\text{nm}} + \sum_i^{\text{Trp,Tyr,Phe}} \epsilon_i^{220\text{nm}} \tag{4}$$

where n is the number of peptide bond units. Figure 5b compares the electron photodetachment yield measured at 220 nm with their absorbance estimated using eq 4 (with $\epsilon_{\text{peptide bond}}^{220\text{nm}}$ and $\epsilon_i^{220\text{nm}}$ given in Table 2). Here, no direct relation between the absorption properties A_i estimated by eqs 1 and 4 and the photodetachment yield is found ($Q = 1.517$). This discrepancy may be due to the estimation of the absorption cross section and/or to the difference between absorption and detachment cross sections. The absorption coefficient is particularly difficult to estimate at 220 nm. First, in solution, the extinction

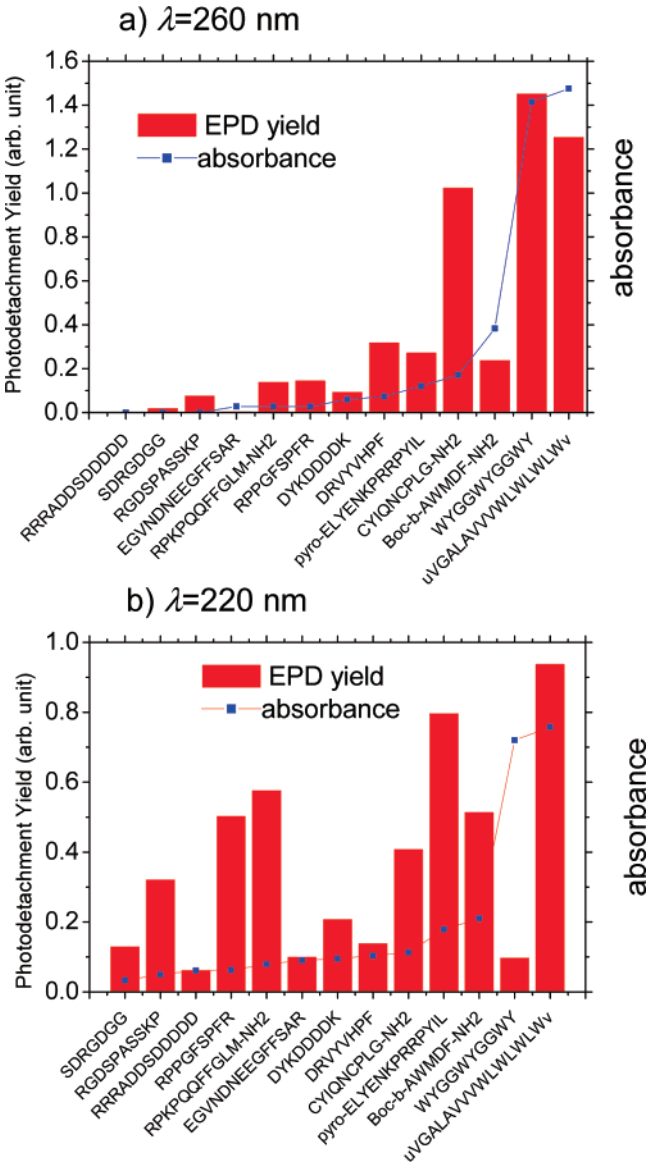

Figure 5. Photodetachment yield (red columns) compared to the estimated absorbance for 13 peptides at $\lambda = 260$ nm (a) and $\lambda = 220$ nm (b). (u and v in gramicidin sequence are respectively for formyl and ethanolamine groups.) A least squared fit method was used for the normalization between electron photodetachment and absorption efficiencies (see text). The irradiation times at 260 and 220 nm were respectively 500 and 1000 ms.

TABLE 2: Molar Extinction Coefficients of Aromatic Amino Acids and the Peptide Bond Unit in Solution at 260 and 220 nm

residue	ϵ (L mol^{-1} cm^{-1}) @ 260 nm	ϵ (L mol^{-1} cm^{-1}) @ 220 nm
Phe	144[a]	710[a]
Tyr (−OH)	612[a]	4312[a]
Tyr (tyrosylate −O$^-$)	1750[b]	4850[b]
Trp	3765[a]	12872[a]
peptide bond unit	0[c]	425[c]

[a] Reference 31. [b] Reference 32. [c] Reference 33.

coefficients strongly depend on the secondary structures of the peptides.[24,30] Second, the absorption cross section can be shifted between gas phase and solution (see Figure 2). The 220 nm absorption is located in the wing of a strong absorption band, and a small shift would induce significant change in the absorption. Due to these two effects, the estimation of the absorption coefficients at 220 nm with eq 2 may be significantly inaccurate.

IV. Conclusion

In summary, we have presented an energy-resolved study of electron photodetachment on peptide dianions. Photodetachment yields of peptides in the gas phase are strongly correlated to their absorption in solution. Within the time scale of our experiment, an electron detachment is observed only if an electronic excitation of the peptide has occurred. Simple energetic considerations allow us to propose a two-step mechanism for the electron detachment: (1) resonant electronic excitation followed by (2) a crossing with an autoionizing state leading to a detachment of the electron. A comparative study of the electron detachment yield for 13 peptides was performed at 260 nm and at 220 nm. At 260 nm, the photodetachment yields follow the absorption efficiencies given by the aromatic amino acid exctinction coefficients deduced from solution data. The electronic excitation corresponds to $\pi\pi^*$ excitation and seems to be weakly sensitive to the sequence and the overall conformation of the peptide. On the contrary, at 220 nm, there is no direct relation between the electron photodetachement yields and solution absorption efficiencies. At 220 nm, the peptide backbone contributes to the total absorption and electron photodetachment yield may be sensitive to the peptide conformation.

Acknowledgment. Dr. A. R. Allouche is gratefully acknowledged for providing us the detachment energies calculated at the DFT level of theory on HCO_2 and aspartic acid.

References and Notes

(1) Wang, X.-B.; Yang, X.; Wang, L. S. *Int. Rev. Phys. Chem.* **2002**, *21*, 473.
(2) Dreuw, A.; Cederbaum, L. S. *Chem. Rev.* **2002**, *102*, 181.
(3) Rienstra-Kiracofe, J. C.; Tschumper, G. S.; Schaefer, H. F.; Nandi, S.; Ellison, G. B. *Chem. Rev.* **2002**, *102*, 231.
(4) Scheller, M. K.; Compton, R. N.; Cederbaum, L. S. *Science* **1995**, *270*, 1160.
(5) Boldyrev, A. I.; Gutowski, M.; Simons, J. *Acc. Chem. Res.* **1996**, *29*, 497.
(6) Wang, X.-B.; Wang, L.-S. *Nature* **1999**, *400*, 245.
(7) Weber, J. M.; Ioffe, I. N.; Bernt, K. M.; Loffler, D.; Friedrich, J.; Ehrler, O. L.; Danell, A. S.; Parks, J. H.; Kappes, M. M. *J. Am. Chem. Soc.* **2004**, *126*, 8585.
(8) Wang, L.-S.; Wang, X.-B. *J. Phys. Chem. A* **2000**, *104*, 1978.
(9) Wang, X.-B.; Ding, C.-F.; Wang, L.-S. *Chem. Phys. Lett.* **1999**, *307*, 391.
(10) Wang, X.-B.; Ding, C.-F.; Wang, L.-S. *Phys. Rev. Lett.* **1998**, *81*, 3351.
(11) Loo, J. A.; Loo, R. R. O.; Light, K. J.; Edmonds, C. G.; Smith, R. D. *Anal. Chem.* **1992**, *64*, 81.
(12) Loo, J. A. *Mass Spectrom. Rev.* **1997**, *16*, 1.
(13) Anusiewicz, W.; Berdys-Kochanska, J.; Czaplewski, C.; Sobczyk, M.; Daranowski, E. M.; Skurski, P.; Simons, J. *J. Phys. Chem. A* **2005**, *109*, 240.
(14) Boxford, W. E.; Dessent, C. E. H. *Phys. Chem. Chem. Phys.* **2006**, *8*, 5151.
(15) Yang, X.; Wang, X.-B.; Vorpagel, E. R.; Wang, L.-S. *Proc. Natl. Acad. Sci. U.S.A.* **2004**, *101*, 17588.
(16) Gabelica, V.; Tabarin, T.; Antoine, R.; Rosu, F.; Compagnon, I.; Broyer, M.; De Pauw, E.; Dugourd, P. *Anal. Chem.* **2006**, *78*, 6564.
(17) Gabelica, V.; Rosu, F.; Tabarin, T.; Kinet, C.; Antoine, R.; Broyer, M.; De Pauw, E.; Dugourd, P. *J. Am. Chem. Soc.* **2007**, *129*, 4706.
(18) Antoine, R.; Joly, L.; Tabarin, T.; Broyer, M.; Dugourd, P.; Lemoine, J. *Rapid Commun. Mass Spectrom* **2007**, *21*, 265.
(19) Kordel, M.; Schooss, D.; Gilb, S.; Blom, M. N.; Hampe, O.; Kappes, M. M. *J. Phys. Chem. A* **2004**, *108*, 4830.
(20) Joly, L.; Antoine, R.; Allouche, A. R.; Broyer, M.; Lemoine, J.; Dugourd, P. *J. Am. Chem. Soc.* **2007**, *129*, 8428.
(21) Talbot, F. O.; Tabarin, T.; Antoine, R.; Broyer, M.; Dugourd, P. *J. Chem. Phys.* **2005**, *122*, 074310.

(22) Ponder, J. W. TINKER Software Tools for Molecular Design,, Version 4.2. Washington University School of Medicine in St. Louis, 2004.

(23) Wang, J.; Cieplak, P.; Kollman, P. A. *J. Comput. Chem.* **2000**, *21*, 1049.

(24) Holzwarth, G.; Doty, P. *J. Am. Chem. Soc.* **1965**, *87*, 218.

(25) Kim, E. H.; Bradforth, S. E.; Arnold, D. W.; Metz, R. B.; Neumark, D. M. *J. Chem. Phys.* **1995**, *103*, 7801.

(26) Danell, A. S.; Parks, J. H. *J. Am. Soc. Mass Spectrom* **2003**, *14*, 1330.

(27) Wang, X.-B.; Vorpagel, E. R.; Yang, X.; Wang, L.-S. *J. Phys. Chem. A* **2001**, *105*, 10468.

(28) Beychok, S.; Breslow, E. *J. Biol. Chem.* **1968**, *243*, 151.

(29) Gunion, R. F.; Gilles, M. K.; Polack, M. L.; Lineberger, W. C. *Int. J. Mass Spectrom. Ion Processes* **1992**, *117*, 601.

(30) Rosenheck, K.; Doty, P. *Proc. Natl. Acad. Sci. U.S.A.* **1961**, *47*, 1775.

(31) Du, H.; Fuh, R. A.; Li, J.; Corkan, A.; Lindsey, J. S. *Photochem. Photobiol.* **1998**, *68*, 141.

(32) Shugar, D. *Biochem. J.* **1952**, *52*, 149.

(33) Goldfarb, A. R. *J. Biol. Chem.* **1953**, *201*, 317.